

MIXED ORBITAL GROUND STATES OF Fe^{2+} IN PRUSSIAN BLUES

A. I. Rykov,¹ J. Wang¹, T. Zhang¹, and K. Nomura²

¹*Mössbauer Effect Data Center, Dalian Institute of Chemical Physics,*

Chinese Academy of Sciences, 457 Zhongshan Road, Dalian 116023, China,

²*School of Engineering, The University of Tokyo, Hongo 7-3-1, 113-8656, Japan,*

(Dated: July 19, 2013)

We report on the mixed-orbital ground state compounds analogous to the mixed-valence ones. Orbital doublet and singlet ground states of the Fe^{2+} ion displayed in Mössbauer spectra of the Prussian blue analogues $\text{A}_y\text{Fe}_{3-y}[\text{Co}(\text{CN})_6]_2 \cdot x\text{H}_2\text{O}$ ($y \leq 1$) are interconverting to each other as temperature changes for $\text{A} = \text{K}, \text{Na}$. Relative weight of orbital singlet ground states increases with lowering temperature. In the alkali-free cobaltcyanides, the Mössbauer spectra are dominated by quadrupole-split doublets of the same origin with a large splitting, characteristic of the Fe^{2+} species coordinated by two (at least) oxygen atoms of water molecules in *cis*-configuration. Single-type octahedral Fe^{2+} coordination is isolated in A-filled cobaltcyanides for $\text{A}=\text{Rb}, \text{Cs}$ to be characterized by the narrower quadrupole spectrum associated with the orbital doublet ground states. Ionic exchange of K for Cs in $\text{KFe}[\text{Co}(\text{CN})_6] \cdot \text{H}_2\text{O}$ results in predominance of the orbital singlet, i.e., in enhanced anisotropy of the Fe^{2+} valence electrons. We found hence that the Fe^{2+} charge distribution can be modified together with crystal size at the step of synthesis owing to distortion isomerism.

PACS numbers: 71.70.-d Level splitting and interactions; 76.80.+y Mössbauer effect;

I. INTRODUCTION

Materials enclosing the transition metal elements are characterized by a wide diversity of ground states whether this be the quantum states of collective electron systems or local states. In latter case, the transitions between disparate ground states of 3d ions can be driven by changes in temperature, chemical doping, or by external stimuli. Phase transitions are thus induced that involve the spin, charge, lattice and orbital degrees of freedom. Charge transfer, spin crossover and linkage isomerism are the three types of transitions requiring a complex elucidation of the roles of corresponding degrees of freedom to be distinguished from each other¹⁻³. The long-range structural aspects display their role via succession of transition steps as they evidence the interconversions between various local states mediated by elastic interactions^{4,5}. Charge transfer from one site to another could be a prerequisite of the concomitant spin-state transition^{6,7}. Orbital degree of freedom is responsible for a long-range-distortion symmetry lowering, provided that orbital ordering is coupled with the mixed-valence charge ordering transition⁸. Orbital ground state reversal⁹⁻¹⁸ is an example of yet another type of transitions strongly coupled to the lattice and, possibly, to some other degrees of freedom. Simultaneous presence of the orbital singlet and orbital doublet ground states, familiar in case of Fe^{2+} ion¹⁹, could be an indication of proximity of such a transition.

Prussian blue (PB) analogues constitute a family of simple cubic compounds which excited a great interest recently owing to the family members exemplifying the spin crossover, charge transfer and linkage isomerism¹⁻³. Here, in the same family, $\text{A}_y\text{Fe}_{3-y}[\text{Co}(\text{CN})_6]_2 \cdot n\text{H}_2\text{O}$ ($y \leq 1$, $\text{A} = \text{K}, \text{Na}, \text{Rb}, \text{Cs}$), we report on mixing and interconverting the orbital ground states of Fe^{2+} .

Metal-organic framework of the PB analogues is formed by the 3d metal cations and the cyanometallate complex anions (of the $[\text{Co}(\text{CN})_6]^{3-}$ -type) arranged into a NaCl-like 3D checkerboard. In major group of these compounds, the valence and spin differ between the states of metal ions occupying the cationic node and the anion core. The framework complex anions are typically having higher valences than the cations, in this case, the framework is bearing a net negative charge, which is balanced either by insertion of alkali (A) cations into the framework interstitials or by spontaneous generation of the large-size vacancies on the anionic nodes. Crystallization and zeolitic water molecules (C-water and Z-water) fill the cavities at the vacant sites of complex anions and A-cations, respectively.

The local electronic configurations are probed by the quadrupole interactions of a ^{57}Fe Mössbauer nuclei sensing the electric field gradient from valent electrons and lattice charges surrounding the Fe^{2+} ion. Mössbauer spectra of ferrous hexacyanocobaltates were reported previously only for the alkali-free phases ($y = 0$)^{20,21}. The spectra can be fitted by two or more quadrupole doublets implying the existence of a number of different states of the high-spin Fe^{2+} ions. Paired doublets, both originating from the cationic sites outside the low-spin complex $[\text{M}(\text{CN})_6]$ were also observed in Mössbauer spectra of some other ferrous hexacyanometallates, e.g., for $\text{M}=\text{Cr}$ ($y = 0$)²². The early Mössbauer study²⁰ has proposed that the water molecules in *cis*- and *trans*- configurations could contribute to the appearance of multiple sites for Fe^{2+} . In case of $\text{M}=\text{Cr}$, the spin-state transition of Fe^{2+} was observed only for $y \neq 0$ ($\text{A}=\text{Cs}$)²³. It was conjectured²³ that filling the structure with A ions induces a stronger ligand field on the Fe^{2+} ion that causes the spin transition. In this study of the local electronic configurations in $\text{AFe}[\text{Co}(\text{CN})_6] \cdot \text{H}_2\text{O}$ ($\text{A} = \text{K}, \text{Na}, \text{Rb}$,

Cs) and related alkali-free form we show that the ligand field stabilizes the singular ground state (orbital doublet) only for A=Cs and Rb. In the cases of A=Na, K, and $y = 0$ we report on the coexisting orbital singlet and orbital doublet ground states for Fe^{2+} and on the inter-conversions between them induced by changes of temperature.

II. EXPERIMENTAL

$\text{RbFe}[\text{Co}(\text{CN})_6] \cdot \text{H}_2\text{O}$ and $\text{CsFe}[\text{Co}(\text{CN})_6] \cdot \text{H}_2\text{O}$ were prepared mixing the 0.025 M aqueous solution of $\text{K}_3\text{Co}(\text{CN})_6$ with 0.025 M solutions of $\text{FeCl}_2 \cdot 4\text{H}_2\text{O}$ in excess of RbCl or CsCl. Similarly synthesized samples in excess of KI and NaCl gave the compounds $\text{K}_{0.8}\text{Fe}_{1.1}[\text{Co}(\text{CN})_6] \cdot 2\text{H}_2\text{O}$ and $\text{Na}_{0.7}\text{Fe}_{1.15}[\text{Co}(\text{CN})_6] \cdot 3\text{H}_2\text{O}$, respectively. The A-free compounds were synthesized from solutions of similar molarity (sample 8 in Table I) and from 10-fold diluted (sample 6). Analytic methods of inductively-coupled plasma and x-ray-fluorescent analysis gave the results consistent with the site occupancies obtained from Rietveld analysis. The same compounds with different crystal size were synthesized for A=Rb and Cs via the ionic exchange using $\text{KFe}[\text{Co}(\text{CN})_6] \cdot 2\text{H}_2\text{O}$ as a sorbent. Transformation of this sorbent into $\text{CsFe}[\text{Co}(\text{CN})_6] \cdot \text{H}_2\text{O}$ was detected by Rietveld analysis and confirmed by analytic techniques.

Table I. Lattice parameters in the precipitated and ion-exchanged hexacyanocobaltates at room temperature.

	Compound	Parameter*, nm
1	$\text{Na}_{0.7}\text{Fe}_{1.15}[\text{Co}(\text{CN})_6] \cdot 3\text{H}_2\text{O}$	1.03278(8)
2	$\text{K}_{0.8}\text{Fe}_{1.1}[\text{Co}(\text{CN})_6] \cdot 2\text{H}_2\text{O}$	1.03115(3)
3	$\text{KFe}[\text{Co}(\text{CN})_6] \cdot \text{H}_2\text{O}$	1.03107(3)
4	$\text{RbFe}[\text{Co}(\text{CN})_6] \cdot \text{H}_2\text{O}$	1.03455(7)
5	$\text{CsFe}[\text{Co}(\text{CN})_6] \cdot \text{H}_2\text{O}$	1.03682(8)
6	$\text{Fe}[\text{Co}(\text{CN})_6]_{0.67} \cdot 5\text{H}_2\text{O}$	1.02778(8)
7	Cs-exchanged (b) at 20°C	1.03628(8)
8	$^{57}\text{Fe}[\text{Co}(\text{CN})_6]_{0.67} \cdot 5\text{H}_2\text{O}$	1.02813(9)

*Refined according to Fig.1 (c) and (d) structure models using the $\text{Fm}\bar{3}\text{m}$ space group.

X-ray Diffraction (XRD) patterns were measured on a PW3040/60 X'pert PRO (PANalytical) diffractometer using Cu K α source. The atomic ratio Fe/Co and K/Co were determined by inductively coupled plasma atomic emission spectrometer (ICP-AES) on an IRIS Interpid II XSP Instrument (Thermo Electron Corporation). The x-ray fluorescent analysis was carried out using the XRF Axios X (PANalytical) spectrometer. The water content in the samples was estimated by thermogravimetric analysis carried out using a Setaram Setsys 16/18 analyser measuring the weight loss in an air flow of 25 ml/min with a heating rate of 10 K/min. Magnetization of the paramagnetic compounds was measured with a SQUID magnetometer in the range between 2 K to 350K.

Mössbauer spectra were measured with a Topologic

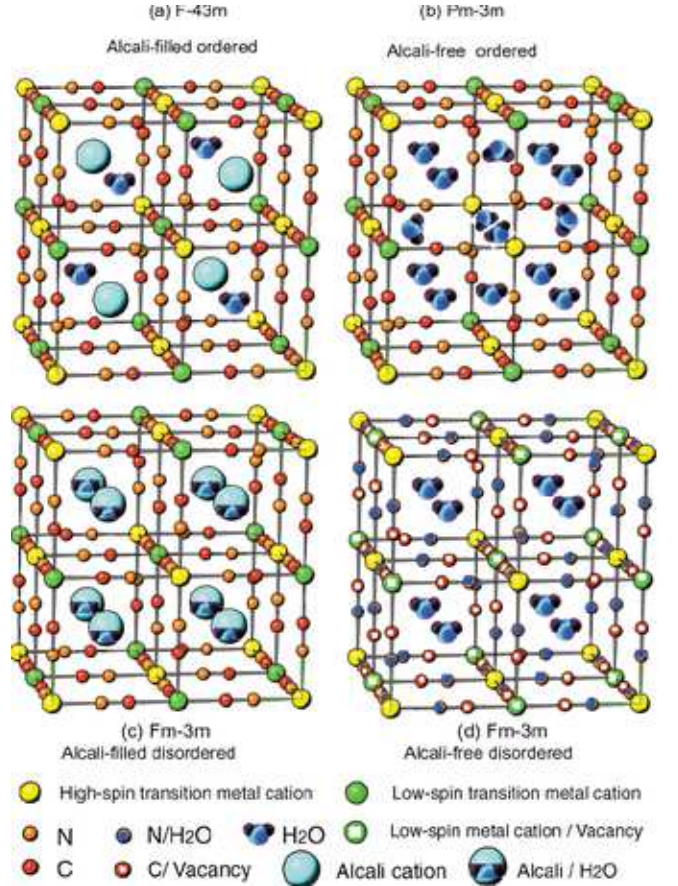


FIG. 1: Crystal structures and symmetry groups of the four modifications of Prussian blue analogues: alkali-filled ordered $\text{F}\bar{4}3\text{m}$ (a), alkali-free ordered $\text{Fm}\bar{3}\text{m}$ (b), alkali filled disordered $\text{Fm}\bar{3}\text{m}$ (c) and alkali-free disordered $\text{Fm}\bar{3}\text{m}$ (d).

500 A spectrometer at the temperatures between 78 K and room temperature. The measurements at heating the sample above room temperature were performed in a Wissel GMBH furnace. Isomer shifts (IS) are reported relative to α -Fe at room temperature.

III. RESULTS AND DISCUSSION

A. Structural considerations

The A-filled and A-free Prussian Blues are two types of the cubic frameworks, described by structure models of Keggin and Miles²⁴ and Ludi²⁵, respectively. Both of them exhibit the variable degrees of randomness in the distribution of the A ions over the framework interstitials and in the distribution of the water-filled anionic vacancies. In both cases, the *random* structures are described by the symmetry group $\text{Fm}\bar{3}\text{m}$. When the A-cations and Z-waters occupy the interstitials in an *ordered* fashion the symmetry turns into $\text{F}\bar{4}3\text{m}$. The $\text{F}\bar{4}3\text{m}$ symmetry appears, for example, in $\text{CsFe}[\text{Cr}(\text{CN})_6] \cdot \text{H}_2\text{O}$ ²³. It means

in the ideal case that the system of framework interstitials splits into two sublattices (1:1), as shown in Fig 1(a). In reality, each of these (1:1) sublattices is not represented by solely A-ions and Z-waters, but occupied just unequally with these two species.

In the A-free structure, another sublattice may split into two subsystems that is the anionic sublattice. When one proceeds from the disordered to ordered placement of anionic vacancies the symmetry turns from $Fm\bar{3}m$ to $Pm\bar{3}m$ giving birth to two dissimilar sublattices²⁶. In the $Pm\bar{3}m$ structure, two born sites are abundant with the ratio of 3:1. Four relevant lattice cells are shown in Fig.1 for the pairs of A-free and A-filled structures.

Rietveld refinements were carried out using the above mentioned four structural models and three symmetry groups known from the literature^{24–27}. These treatments have shown that the most symmetric $Fm\bar{3}m$ model is sufficient to fit all the observed reflections. When fitted with lower symmetries the XRD least-square analysis has resulted in stagnant goodness of fit, unimproved, despite larger number of fitting parameters. The intensity ratio I_{200}/I_{220} changes dramatically when K, Rb or Cs ions enter into the structure, as reported previously²⁸. The change becomes very large as the number of electrons in an alcali ion increases, allowing for Cs a rough estimation of its content even prior to Rietveld analysis.

The refined lattice parameters at ambient temperature are listed in Table I. In all compounds, the lattice parameter is close to that of the low-spin phase of $CsFe[Cr(CN)_6] \cdot H_2O$ ²³, however, it is found from magnetic measurements that the addressed in Table I compounds enclose the Fe^{2+} ions in the high-spin state that is unchanged down to 2 K.

B. Doublet and singlet orbital ground states of Fe^{2+} in PB analogues

1. Splitting the d-orbital energy level in anisotropic environment

In the fully A-filled PB analogues, the Fe^{2+} ions are coordinated with six nitrogens, however, at partial filling at least one C-water molecule enters the first coordination sphere of Fe^{2+} . From the combined scheme of compensating the charge misbalance between Fe^{2+} cations and $Co(CN)_6^{3-}$ anions this is evidently the case of our samples (Table I). Electronic configuration of a high-spin d^6 ion implies only one electron extraneous with respect to isotropic half-closed d-shell composed of five spins-up electrons. In an octahedral environment, the group of three t_{2g} orbitals is available for this sixth electron. We show in Fig. 2 the orientations of these orbitals relative to the water molecule.

In case of octahedral high-spin Fe^{2+} , the magnetic susceptibility of an ion is contributed by the orbital motion of the t_{2g} valence electron that is added to the spin $S=2$ through the spin-orbit coupling. The valence contri-

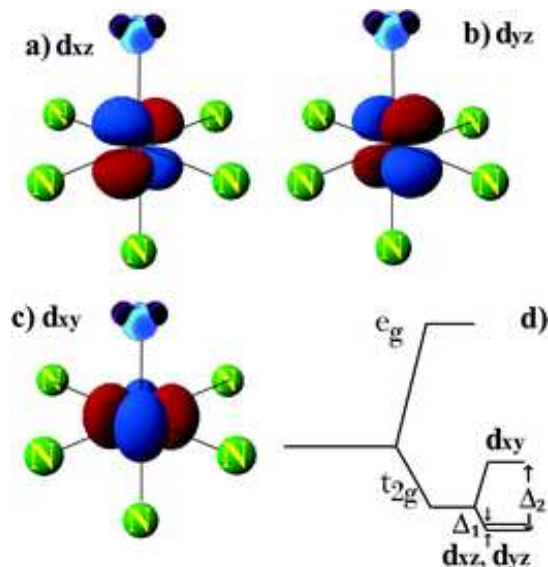


FIG. 2: Formation of the orbital doublet ground state of Fe^{2+} in the "5+1" environment. In a Prussian Blue analogue, the valence spin-down electron clouds are depicted for the Fe^{2+} species coordinated by 5 nitrogens and one water molecule. It is shown that two orbitals of the t_{2g} group (d_{xz}, d_{yz}) retain the equivalent energy (a,b), whereas the third one (c) splits off upwards. A single spin-down electron occupies the double-degenerate level forming the doublet orbital ground state.

bution of the electric field gradient (EFG) is predominant and exceeds the lattice EFG term by an order of magnitude^{29,30}. The t_{2g} group is the source of valence term of EFG that is the main contribution of the observed quadrupole splitting.

One of the orbitals of the t_{2g} group in Fig. 2 (a,b,c) is perpendicular to the direction pointing towards the water molecule. Corresponding energy level would not be affected by the ligand replacement. The lobes of two other orbitals (d_{xz} and d_{yz} in Fig.2) are at 45° with respect to oxygen direction. Owing to reduced repulsion between oxygen and d_{xz} or d_{yz} electrons corresponding levels would have lower energy. In the ground state of Fe^{2+} ion, these d_{xz} and d_{yz} orbitals share the sixth d-electron (spin-down electron), while five spin-up d-electrons span isotropically. The third (d_{xy}) orbital would split off its energy level upwards from the ground state, formed by two degenerate d_{xz} and d_{yz} orbitals as shown in Fig. 2(d). The Fig. 2 (d) is relevant to zero spin-orbit coupling. In case of combined effect of an axial field and of spin-orbit interaction nine energy levels are produced, namely three singlets and six doublets³¹.

2. Magnetic properties of the high-spin Fe^{2+} ions in the distorted octahedral crystal field

In the hexacyanocobaltates, where the high-spin Fe^{2+} species are surrounded by a low-spin complex anions

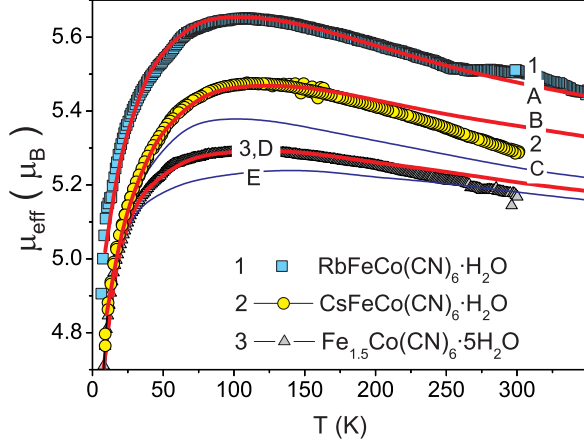


FIG. 3: Experimental and theoretical curves of $\mu_{\text{eff}} = 2.83\sqrt{\chi_{\text{mol}}T}$ vs. temperature for three compounds (4, 5 and 6 in Table I). The solid curves are from the theory³³ for the parameters (A): $\Delta_1 = 190 \text{ cm}^{-1}$, $\Delta_2 = 0$, $\lambda = 63 \text{ cm}^{-1}$, $\kappa = 1$; (B) $\Delta_1 = 210 \text{ cm}^{-1}$, $\Delta_2 = 0$, $\lambda = 70 \text{ cm}^{-1}$, $\kappa = 0.8$; (C) $\Delta_1 = 170 \text{ cm}^{-1}$, $\Delta_2 = 0$, $\lambda = 55 \text{ cm}^{-1}$, $\kappa = 0.7$; (D) $D = \sqrt{0.4 \cdot C^2 + 0.6 \cdot E^2}$; (E) $\Delta_1 = \Delta_2 = 350 \text{ cm}^{-1}$, $\lambda = 70 \text{ cm}^{-1}$, $\kappa = 0.6$.

$[\text{Co(III)(CN)}_6]^{3-}$, the Fe^{2+} site is a single source of paramagnetism. Orbital motion contributing to the magnetic moment of Fe^{2+} is unfrozen in the extent determined by the degree of bonding covalence. Ligand replacement affects the degree of valent electron delocalization. Variation of magnetic moment of Fe^{2+} ions over the sample is expected caused by the effect of a number of C-waters entering the first coordination sphere of Fe^{2+} . There appears a distribution of the Fe^{2+} ions over the number of the C-water ligands. For the magnetic measurements the samples 4-6 of the Table I were selected. The compounds $\text{RbFe}[\text{Co(CN)}_6] \cdot \text{H}_2\text{O}$ and $\text{CsFe}[\text{Co(CN)}_6] \cdot \text{H}_2\text{O}$ were selected because they are fully A-filled, enclosing only the Z-water, and showing the single-site Mössbauer spectra. As a counterpart from the opposite family the compound $\text{Fe}[\text{Co(CN)}_6]_{0.67} \cdot 5\text{H}_2\text{O}$ was selected (the sample No. 6). A convenient method to display the results of magnetic measurements is to plot the experimental curves $\mu_{\text{eff}}(T)$ fitted with theoretical ones³¹⁻³⁴. Accordingly, in Fig. 3, the experimental data (1) and (2) for $\mu_{\text{eff}}(T)$ are matched to a single set of fitting parameters (δ, λ, κ). The data (3) are approximated by a mean squared $\mu_{\text{eff}} = \sqrt{A_1\mu_{\text{eff}}^2(1) + A_2\mu_{\text{eff}}^2(2)}$ with two magnetic moments $\mu_{\text{eff}}(1)$, $\mu_{\text{eff}}(2)$ and abundances A_1 , A_2 adjusted to the parameters of subspectra observed in corresponding Mössbauer spectra.

From the theory of magnetic properties of transition metal ions in low-symmetry ligand field³¹⁻³⁴ the $\mu_{\text{eff}}(T)$ is predicted to culminate around 100 K exceeding the spin-only value of $4.9\mu_B$ and depending on the crystal-field splitting energy, the energy of spin-orbit coupling λ ,

and the orbital reduction factor κ . The results tabulated in the reports of two groups^{33,34} coincide³⁵.

The curves $\mu_{\text{eff}}(T)$ can be described in terms of low-temperature dip (below maximum), the negative slope (above maximum), and the overall level. The width of the low- T dip in the $\mu_{\text{eff}}(T)$ curves scales with λ , therefore, the value of λ can be most accurately fitted, using the accurate claim that we can exclude mixing antiferromagnetism into such a low- T dip. On the other side, the negative slope of the μ_{eff} vs. T curve is steeper when the orbital doublet is lowest ($\Delta_2 = 0$). In this case (Rb and Cs-samples), large slope absolute value evidences the orbital doublet ground state. The slope is almost unvaried with Δ_1 , while the level of μ_{eff} depends strongly on Δ_1 . However, the level of μ_{eff} depends also strongly on κ . The correlation between these two dependencies reduces much the accuracy of determination of Δ_1 . Nevertheless, the choice between the cases of $\Delta_2 = 0$ and $\Delta_1 = \Delta_2$ is unambiguous.

With increasing the degree of t_{2g} electron delocalization both values of λ and κ are reduced from their ideal free-ion values of $\lambda_0 = -100 \text{ cm}^{-1}$ and $\kappa_0 = 1$, respectively³⁴. A concomitant reduction of λ/λ_0 and κ/κ_0 in a series of coordination compounds was evidenced by Figgis et al³⁴. Our results in Fig. 3 confirm such a correlated reduction, except in Rb-based compound. However, if one assume that the molar weight of our sample is slightly reduced by Rb-deficiency, the value of κ would be reduced as well. The deficiency of 0.06 (three times smaller than in our $\text{K}_{0.8}\text{Fe}_{1.1}[\text{Co(CN)}_6] \cdot \text{H}_2\text{O}$ sample) would correspond to the reduction of κ from 1 to 0.8. In the samples 5 and 6, the observed $\mu_{\text{eff}}(T)$ decreases with increasing temperature even more steeply than does the maximally steep theoretical curve (Fig. 3). This result can be explained³¹ by the change of the covalence degree with temperature as the overlap between the iron(II) 3d- and ligand charge clouds changes owing to thermal expansion³¹.

3. Temperature dependence of quadrupole splitting in A-filled cobalticyanides ($A = \text{Na}, \text{K}$):

We observe two doublets, both of them having the temperature-dependent quadrupole splitting. In addition, the ratio of doublet areas is also strongly temperature-dependent. The values of chemical shifts for both doublets in Fig. 4 are in the range 1.1 mm/s to 1.15 mm/s allowing us to identify both doublets with the high-spin Fe^{2+} . A tiny spectral asymmetry indicates a trace of oxidized (Fe^{3+}) component.

The external doublet is dominating at low temperatures. As the temperature is raised an inverted doublet area ratio is observed. Mössbauer spectra suggest that the triple degeneracy of t_{2g} is lifted over either in favor of the orbital singlet or in favor of orbital doublet ground states. The charge distribution is less anisotropic when the spin-down electron is shared between two orbitals as

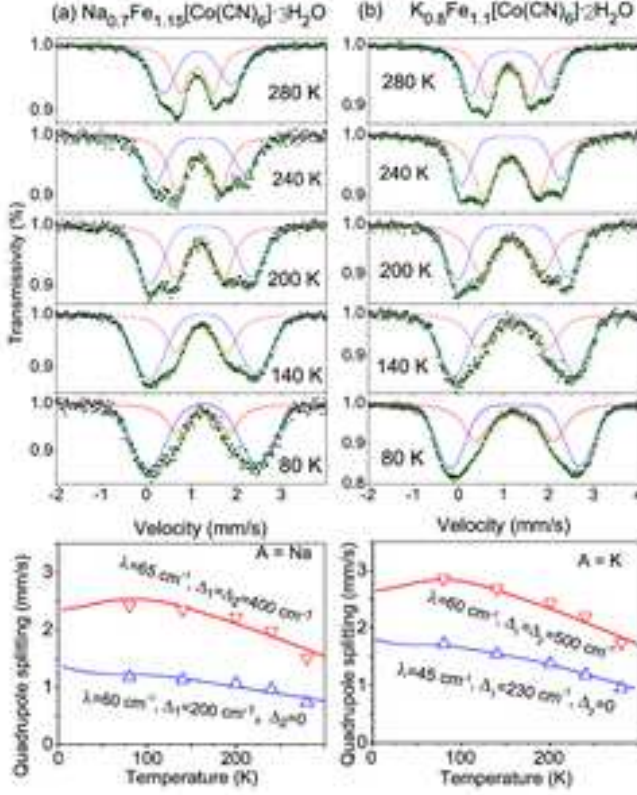


FIG. 4: Mössbauer spectra of the A-filled ferrous hexacyanocobaltates for A=Na and K in temperature range between 80 K and 280 K. In the bottom panels, the experimental temperature dependences of the quadrupole splitting determined from least-squares fitting the Mössbauer spectra are shown by triangle symbols. The solid lines represents $\Delta E_Q(T)$ fitted using the reduction factors $F'(T)$ from Ref.³⁷ with the parameters values of λ , Δ_1 and Δ_2 indicated. For the sake of clarity the minor site (cf. 2 to 5% in Tables II and III) is not shown in the spectra partitioning. Plausible origin of this site occupied by iron in oxidized form (Fe^{3+}) is discussed in Sec.III D.

shown in Fig. 2. We ascribe such a charge state to the internal quadrupole doublet of Fig.4.

Larger charge anisotropy originates from localizing the sixth electron of Fe^{2+} on a single d -orbital (external QS doublet). From the QS ratio the valence EFG term is expected to be twice larger for the orbital singlet than for the orbital doublet. The literature overview confirms indeed that in Fe^{2+} the orbital singlet produces twice larger quadrupole splitting than the orbital doublet ground state^{9–19,30,36,37}.

In the bottom of Fig. 4, we fitted the curves $\Delta E_Q(T)$ using the approach developed by Ingalls³⁷. The crystal-field splitting, the spin-orbital interactions, the lattice term and covalency effects are taken into account in a step-by-step procedure³⁸ allowing to estimate the triplet t_{2g} splitting energies Δ_1 , Δ_2 , the spin-orbit coupling con-

stant λ scaled-down by covalency effects from the free-ion value of 100 cm^{-1} , and the lattice term ΔE_{latt} . In the first step, the so-called preliminary results³⁸ were derived from fitting the curves $\Delta E_Q(T)$ with the theoretical expression^{37,38}:

$$\Delta E_Q(T) = \Delta E_Q^0 \frac{(1 + e^{\frac{-2\Delta_1}{k_B T}} + e^{\frac{-2\Delta_2}{k_B T}} - e^{\frac{-\Delta_1}{k_B T}} - e^{\frac{-\Delta_2}{k_B T}} - e^{\frac{-(\Delta_1+\Delta_2)}{k_B T}})^{\frac{1}{2}}}{1 + e^{\frac{-\Delta_1}{k_B T}} + e^{\frac{-\Delta_2}{k_B T}}} \quad (1)$$

Here $\Delta E_Q^0 = (4/7)e^2Q\langle r^{-3} \rangle$ is the quadrupole splitting at zero temperature, which is for Fe^{2+} as high as 4 mm/s ³⁸ or even 4.5 mm/s ³⁷. The Eq.(1) shows that the value of ΔE_Q^0 is reached at $T = 0$ if $\Delta_1 = \Delta_2$ (orbital singlet) but only the value of $\Delta E_Q^0/2$ is reached at $T = 0$ if $\Delta_2 = 0$ (orbital doublet). The preliminary fitting results imply the orbital doublet state for the inner Mössbauer doublet and the orbital singlet state for the outer Mössbauer doublet. Next step of the fitting procedure consist of taking into account the spin-orbit coupling λ . Covalence effects reduce the value of λ compared to the free-ion value of $\lambda_0 \approx -100 \text{ cm}^{-1}$. In this approximation, the Boltzmann distribution of the valence electron [Eq.(1)] over three levels must be replaced with that over nine levels³¹. We used in Fig.4 the theoretical results reported in Figs. 3 and 5 of the Ingall's work³⁷, assuming an axially symmetric local distortions of the FeN_6 octahedra within the entirely cubic structure.

Finally, it is tempting to take into account the temperature-independent lattice term. Most frequently the lattice term is opposite in sign to the valence term and smaller by an order of magnitude²⁹. If the lattice term is subtracted from valence term, the overall $\Delta E_Q(T)$ slope would decrease, thus producing the underestimate of the crystal-field splitting. The contribution ΔE_Q^{latt} of $\sim 10\%$ of ΔE_Q^0 leads to the underestimate of Δ_1 of the order of λ . Lacking the calculation of lattice sums we assumed $\Delta E_Q^{\text{latt}} = 0$ in Fig.4, however, if the ratio $\Delta E_Q^{\text{latt}}/\Delta E_Q^0$ is indeed ≈ -0.1 , then the experimental $\Delta E_Q(T)$ curves may be steeper than the theoretical ones. The divergence of this type is observed in all $\Delta E_Q(T)$ curves of Fig. 4. At approaching 300 K the experimental $\Delta E_Q(T)$ curves become very steep. There could exist, however, other source of such behavior. Yet another possibility is the steep change $\Delta E_Q(T)$ in a proximity of a phase transition^{17,18}, to be sought in these compounds presumably above 300 K. Also, one may attribute the narrow doublet to a large fraction of the supercooled high-temperature phase supposing the high- and low-temperature phases isostructural. Indeed, from XRD no evidence of biphasic character of samples were seen. However, if the transition

is glasslike in its nature, a single phase with disordered cubic structure may be hosting the residual spatial inhomogeneity that implies the mixed orbital ground states coexisting in a way by which different local structures coexist in a glass.

Thermally-induced change of areas of two Mössbauer doublets shows that the population of orbital doublet states grows with increasing temperature. It appears that different local distortions substitute for one another with preserving the global cubic symmetry. This gives us a reason to believe that the coexisting orbital states originate from the *local* distortions of the FeN_6 octahedra that may have either static or dynamic character. In the low-temperature region, the orbital singlet is lowest because the specific distortion of the FeN_6 octahedra might be dynamically more stable. With increasing temperature these polyhedra repose more time in a state of converse distortion. The latter hosts the more isotropic distribution of the Fe^{2+} valence electrons. Dynamic equilibrium shifts towards the reduced electronic anisotropy with increasing temperature. Therefore, the orbital doublet states appear to be partly thermally-induced.

Table II. Parameters of Mössbauer spectra (Fig. 4) in $\text{Na}_{0.7}\text{Fe}_{1.15}[\text{Co}(\text{CN})_6]\cdot 3\text{H}_2\text{O}$: isomer shift (IS) δ , quadrupole splitting (QS) ΔE_Q , linewidths Γ (mm/s), and spectral abundance (%).

T (K)	δ (mm/s)	ΔE_Q (mm/s)	Γ (mm/s)	%
280K	1.142(2)	1.56(1)	0.48(1)	44
	1.110(2)	0.82(1)	0.46(1)	51
	0.46(1)	0.3(2)	0.27(2)	5
240 K	1.161(8)	2.06(2)	0.50(2)	40
	1.168(2)	0.99(3)	0.51(2)	54
	0.35(3)	0.5(2)	0.4(1)	6
200 K	1.209(3)	2.25(1)	0.54(2)	50
	1.169(4)	1.19(1)	0.56(2)	46
	0.4(1)	0.5(2)	0.4(4)	3
140 K	1.218(2)	2.467(9)	0.67(1)	65
	1.240(3)	1.287(1)	0.51(1)	31
	0.5(1)	0.5(2)	0.5(3)	4
80 K	1.236(6)	2.63(3)	0.69(2)	62
	1.283(8)	1.47(3)	0.58(3)	35
	0.5(1)	0.5(2)	0.4(2)	3

Orbital-ground-state reversal in high-spin Fe^{2+} compounds has been a well-known phenomenon since the pioneering work of Dézsi and Keszthelyi⁹, in which a pair of doublets was observed in $\text{Fe}(\text{ClO}_4)_2\cdot 6\text{H}_2\text{O}$ within a rather narrow temperature interval. It was argued in this case, that two different orbital ground states coexists within the transition range owing to the first-order phase transition¹⁰. In this system, the transition was observed by calorimetry, neutron scattering and magnetic susceptibility measurements^{40–42}. Order-disorder transformation in the remote perchlorate ion bonding system

built up of hydrogen bonds was speculated to underlie the crystallographically undetected second-order transition switching the FeO_6 octahedra from compression to elongation along the trigonal axis¹¹. In the isostructural fluoroborate hydrate, Brunot¹⁷ observed not so precipitous change in hydrogen bond dynamics and deduced an inference of a different transition mechanism. The temperature- and pressure-driven orbital ground state reversal phenomena were proven to occur at the first-order phase transitions in iron(II) fluorosilicate hydrate^{15,16}. In thiourea high-spin $\text{Fe}(\text{II})$ compound, no direct evidence of phase transition was found, while singlet and doublet orbital ground states were found to coexist in a wider temperature range^{12–14}. The authors ruled out the interpretation based on classical phase transition after they have conducted the kinetic study^{13,14} that allowed them to specify the transforming system as an intermediate between fully homogeneous and biphasic heterogeneous.

Table III. Parameters of Mössbauer spectra (Fig. 4) in $\text{K}_{0.8}\text{Fe}_{1.1}[\text{Co}(\text{CN})_6]\cdot 2\text{H}_2\text{O}$: isomer shift (IS) δ , quadrupole splitting (QS) ΔE_Q , linewidths Γ (mm/s), and spectral abundance (%).

T (K)	δ (mm/s)	ΔE_Q (mm/s)	Γ (mm/s)	%
280K	1.135(2)	1.76(1)	0.44(1)	44
	1.098(2)	1.007(7)	0.468(8)	54
	0.4(1)	0.3(2)	0.4(2)	2
240 K	1.173(2)	2.207(8)	0.38(2)	36
	1.152(2)	1.185(9)	0.59(1)	62
	0.4(1)	0.5(2)	0.4(1)	2
200 K	1.204(3)	2.45(1)	0.47(2)	44
	1.182(5)	1.19(1)	0.62(2)	54
	0.4(2)	0.5(2)	0.6(4)	2
140 K	1.234(3)	2.68(2)	0.63(2)	62
	1.229(7)	1.54(3)	0.60(3)	37
	0.5(2)	0.5(2)	0.7(3)	1
80 K	1.260(6)	2.86(2)	0.65(2)	60
	1.253(1)	1.72(2)	0.66(3)	39
	0.5(2)	0.5(2)	0.7(3)	1

In the same way, we avoid interpreting the data on Fig. 4 as a classical thermodynamic first-order or second-order phase transition such as phonon-mode condensation. In the compounds of the PB family, the ubiquitous cubic porous framework allows for variable site and cell symmetries to be accommodated (cf. structures in Fig.1). As the steric hindrances released in low-density frameworks the coherence in atomic displacements ceases to exist. Additional factor preventing the cooperativity of the local distortions is the disorder related to incomplete A-filling.

As temperature decreases we observe in Tables II and III that the linewidths of both major doublets increases.

This is because each of the Mössbauer doublets is contributed by several Fe^{2+} sites with different composition of the 1st coordination sphere and with difference of positioning relative to each other of the N and H_2O ligands. Depending on the number and isomeric configuration (trans, cis) of the H_2O ligands around Fe^{2+} site the site contributes either to orbital doublet or to orbitals singlet ground states. Two Mössbauer doublets correspond to two types of the ground state. Therefore, the values of parameters displayed on Fig. 4 ($\Delta_1, \Delta_2, \lambda$) have the meaning of averages over the orbital singlet and orbital doublet ground states. Subtle differences between the crystal-field and spin-orbit parameters of the particular environments give rise to the low-temperature linewidth broadening of both doublets. Next, we classify all the possible ligand configurations by the manner in which the d-orbitals are filled depending on the symmetry of environment.

4. Classification scheme of the Fe^{2+} sites by the symmetry of environment

Our Rietveld refinements in both A-filled and A-free series of cobalticyanides have revealed that their structures are best described by the symmetry $\text{Fm}\bar{3}\text{m}$, allowing for the Fe^{2+} ion to have a number of different coordination environments. The Fe^{2+} sites can be classified by the number and configuration of N-ligands replaced with H_2O . In these Fe^{2+} sites, the lowest in energy state depends on the H_2O inclusion in first coordination sphere, however, when H_2O is not included, the ground state is determined by the local distortion. Owing to so-called distortion isomerism¹² the ground state becomes not uniquely defined. Shown in Fig.5 are the cases of distortion isomerism (a), orbital singlet (b), and orbital doublet (c).

The distortion isomerism is the phenomenon closely related to the inability for the sixth (spin-down) electron to be distributed isotropically over the triply degenerate t_{2g} orbital. Such an overmuch triple degeneracy is universally lifted over by a local distortion of one or another type. In a FeN_6 octahedron, the compression along tetragonal axis would stabilize the orbital singlet lowest (a-1), while elongation along tetragonal axis stabilizes the orbital doublet as a ground state (a-2). Opposite effects are expected for the compression and elongation along the trigonal axis of the octahedron¹⁴. Self-coupling between electron localization and local distortion eliminates the case of zero EFG valence term that is never observed.

This physical picture is a key to understanding the temperature variation of the abundance of two Mössbauer doublets in Fig. 4. Assuming that the 6N-coordinated Fe^{2+} sites are contributing to both doublets, we observe that the relative abundance of the orbital doublet and orbital singlet states is varying with temperature owing to varied lattice distortion. Matsuda et

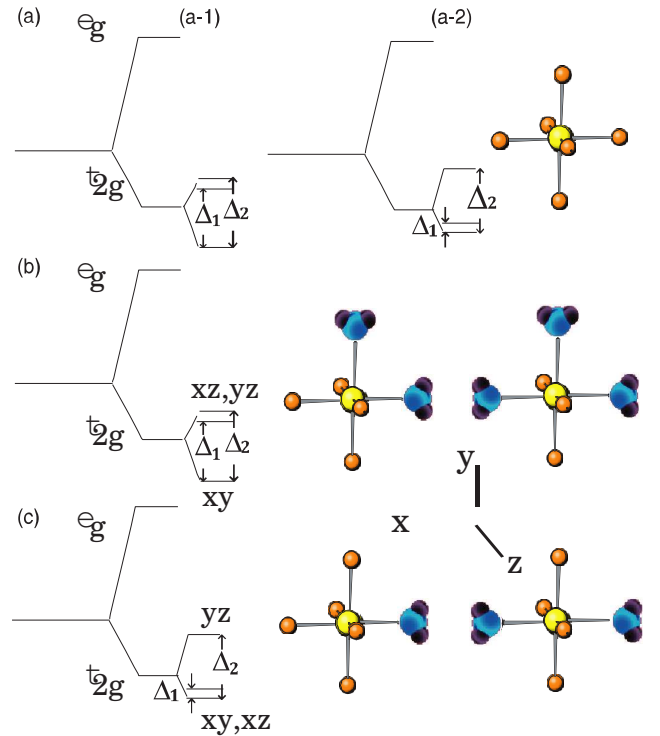


FIG. 5: Energy level diagrams and corresponding coordinations for the orbital singlet (a-1) and (b) and orbital doublet (a-2) and (c) ground states of the Fe^{2+} ion in ferrous hexacyanocobaltate. In a-1 (a-2) the diagram of level splitting for the distorted FeN_6 octahedron is shown for the elongation (compression) along tetragonal (trigonal) axis.

al³⁹ have reported that the PB lattice possess an intrinsic instability with respect to rotations of the rigid units of the $[\text{Co}(\text{CN})_6]^{3-}$ -type. The rotational displacements generate spontaneously to stabilize the excited charge-transferred states, which arises owing to strong lattice-electron coupling. The same rotational displacements cause also the negative thermal expansion³⁹. Recently, the thermal expansion in $\text{Fe}_3[\text{Co}(\text{CN})_6]_2 \cdot n\text{H}_2\text{O}$ was reported to be indeed negative, at least above 200 K⁴³.

We observe thus that the orbital ground state reversal accompanies the distortion isomerism. One or another of coexisting distortion isomers prevails in a particular temperature range. Largest charge anisotropy occurs at lower temperatures owing to localizing the sixth electron of Fe^{2+} on a single d -orbital. The charge distribution is less anisotropic at higher temperatures when the spin-down electron is shared between two orbitals. The temperature variation of the abundance of two Mössbauer doublets is very smooth as the distortions are local and broadly distributed.

With decreasing the content of A-ions the anionic vacancies (water-filled pores) are generated for charge compensation. When the pore concentration is small only populated are the Fe^{2+} sites which contain one H_2O ligand as shown in Figs. 2 and 5(c). Two pores in a vicinity

of a Fe^{2+} species occur either in *trans*- or in *cis*- configurations. Consider in Fig. 5(c), for example, the ground state of the *trans*- Fe^{2+} . If we denote by x the direction from the central Fe^{2+} ion towards two *trans*- H_2O ligands then the lobes of both xy and xz orbitals would be pointing to directions having an angle of 45° with the x axis. The lobes of the third t_{2g} orbital (yz) would be pointing to the direction orthogonal to the x -axis. Therefore the ground state of the Fe^{2+} ion in such $\text{FeN}_4(\text{H}_2\text{O})_2$ octahedron would be the orbital doublet. This is the same ground state as shown in Fig. 2 for the Fe^{2+} ion in the $\text{FeN}_5\text{H}_2\text{O}$ octahedron with single water in first coordination sphere. Orbital singlet in Fig. 5(b) is the ground state corresponding to the *cis*-configuration of $\text{FeN}_4(\text{H}_2\text{O})_2$ and to the octahedron with three in-plane waters.

The H_2O placement into the first coordination sphere of Fe^{2+} suppresses the distortion isomerism and stabilizes a singular ground state of Fe^{2+} . In our samples $\text{Na}_{0.7}\text{Fe}_{1.15}[\text{Co}(\text{CN})_6]\cdot 3\text{H}_2\text{O}$ and $\text{K}_{0.8}\text{Fe}_{1.1}[\text{Co}(\text{CN})_6]\cdot 2\text{H}_2\text{O}$ the density of anionic vacancies is rather small and the population of the Fe^{2+} ions surrounded by two vacancies is also small. In these samples the inner doublet comes from the Fe^{2+} orbital doublet ground state associated with the $\text{FeN}_5\text{H}_2\text{O}$ octahedron and with one of distortion isomers of FeN_6 . The outer doublet comes mainly from another distortion isomer of FeN_6 having the orbital singlet ground state.

5. A-filled cobalticyanides ($A=\text{Rb}, \text{Cs}$)

Another manifestation of distortion isomerism is the difference between the Mössbauer spectra of the A-filled cobalticyanides obtained for Rb and Cs by two different procedures. Using the standard technique, the A-filled cobalticyanides were obtained by precipitation method. These compounds have demonstrated the single-component Mössbauer spectra (a) and (b) in Fig. 6, identified with orbital doublet ground state. On the other hand, when the method of ionic exchange was applied to replace K by Cs in $\text{KFe}[\text{Co}(\text{CN})_6]\cdot \text{H}_2\text{O}$, the second QS subspectrum, identified with the orbital singlet, did not disappear. On the contrary, we observed the strong enhancement of the outer doublet with $\Delta E_Q = 1.8$ mm/s, from 32% to 64%. In addition, there appears a component (13%) with extremely large ΔE_Q of 3 mm/s. It is assigned to another orbital singlet state with larger energy level splitting parameters Δ_1 , Δ_2 . The difference between two external doublets of the sample (d) is a manifestation another type of distortion isomerism unrelated to switching between different orbital ground states⁴⁴.

Rietveld refinements resulted in similar compositions for two different syntheses. The intensity of x-ray diffraction has very similar patterns, except linewidth difference. Larger-size crystallites of $\text{CsFe}[\text{Co}(\text{CN})_6]\cdot \text{H}_2\text{O}$ are obtained via ionic exchange. In this method, the crystal size of $\text{CsFe}[\text{Co}(\text{CN})_6]\cdot \text{H}_2\text{O}$ is determined by the size

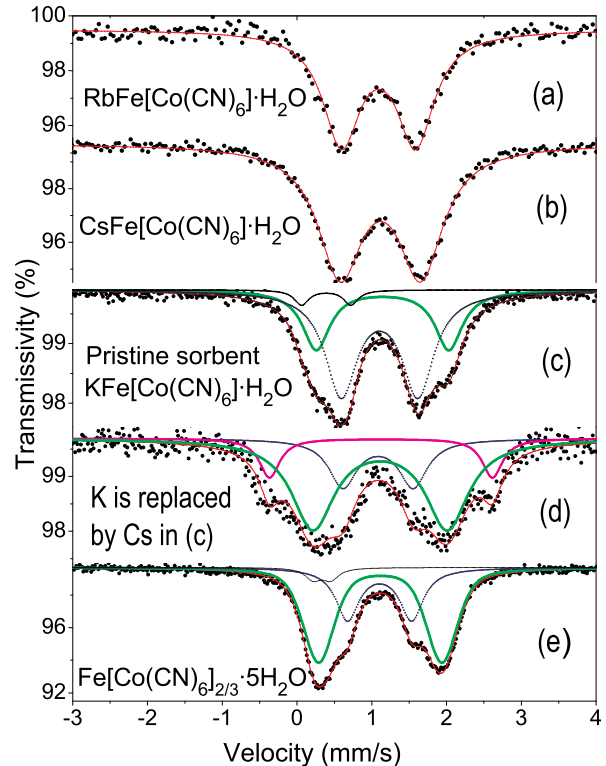


FIG. 6: Mössbauer spectra of the A-filled ferrous hexacyanocobaltates obtained in three different procedures: precipitation (a-c,e), and ionic-exchange (d). The spectra fitting parameters are listed in Table II.

of the $\text{KFe}[\text{Co}(\text{CN})_6]\cdot \text{H}_2\text{O}$ precursor crystals. The target compound $\text{CsFe}[\text{Co}(\text{CN})_6]\cdot \text{H}_2\text{O}$ with such large crystals could not be obtained by the standard method of precipitation from a solute. Despite of similarity of the x-ray patterns, the QS of the ion-exchanged and precipitated samples of $\text{CsFe}[\text{Co}(\text{CN})_6]\cdot \text{H}_2\text{O}$ indicates that the valent spin-down electron has a very different distributions over the orbitals of t_{2g} group (Table IV).

Table IV. Parameters of Mössbauer spectra (Fig. 6) in as-synthesized (a-c) and (e) and Cs-sorbed(d) hexacyanocobaltates: isomer shift (IS) δ , quadrupole splitting (QS) ΔE_Q , linewidths Γ (mm/s), and spectral abundance (%).

Compound	δ (mm/s)	ΔE_Q (mm/s)	Γ (mm/s)	%
(a):RbFe[Co(CN) ₆] ·H ₂ O	1.091(5)	0.992(8)	0.60(1)	100
(b):CsFe[Co(CN) ₆] ·H ₂ O	1.116(3)	1.077(4)	0.71(1)	100
(c):KFe[Co(CN) ₆] ·H ₂ O	1.144(3)	1.77(1)	0.44(2)	32
	1.104(2)	1.03(1)	0.52(2)	64
	0.39(1)	0.66(2)	0.23(3)	5
(d): ion-exchanged K for Cs in (c)	1.111(5)	1.80(3)	0.69(4)	64
	1.084(9)	0.94(3)	0.45(4)	23
	1.123(8)	2.98(2)	0.33(4)	13
(e):Fe[Co(CN) ₆] _{2/3} ·5H ₂ O	1.114(2)	1.65(1)	0.45(1)	64
	1.104(2)	0.86(1)	0.38(1)	31
	0.33(1)	0.23(2)	0.26(3)	5

We observe in the standard (not ion-exchanged) compounds that only one type of the octahedron distortion is preferred when the large-size A-ions occupy the interstitials, and this type of distortion stabilizes the orbital doublet lowest. On the other hand, in the case of A=K or A=Na the appearance of the outer doublet comes into play. In this series of PB analogues, several related aspects of structure and properties turn out to be A-size-dependent. Whereas in the case Cs(Rb)-containing PB analogue compounds the Cs(Rb) ions are situated in the centers of the interstitial cubes, in the case of some K(Na)-containing compounds the K(Na) ions are reported to be eccentrically located⁴⁵. The mobility of alkali metal ions in the channels of the hexacyanometalate structure decrease dramatically with increasing the alkali ionic radius⁴⁵. The irreversible fixation of the less mobile ions ensures the Cs-selectivity for the cobalticyanide sorbents, allowing the ionic exchange to be used in practice for ¹³⁷Cs removal from radioactive wastes^{46,47}.

Although rather large linewidths were observed in the $\gamma=1$ compounds (cf. in Table IV $\Gamma = 0.6$ for A=Rb and $\Gamma = 0.7$ for A=Cs), there is no doubts in attribution of the whole Mössbauer spectra to the orbital doublet ground states. In these cases, the XRD linewidths associated with the smallness of crystal size²⁸ and the Mössbauer linewidths correlate well to each other. The distribution of EFG tensor component values that causes the line broadening arises from the small size of crystals. These compounds contains only the Z-water molecules, therefore, they are closer to anhydrous salts rather than to crystal hydrates wherein the crystallization water helps the precipitation of larger crystals. Similarly large Mössbauer linewidths were observed previously by Kosaka et al²³ in the high-spin phase of the analogous chromate compound CsFe[Cr(CN)₆]_{2/3}·H₂O devoid of crystallization water as well.

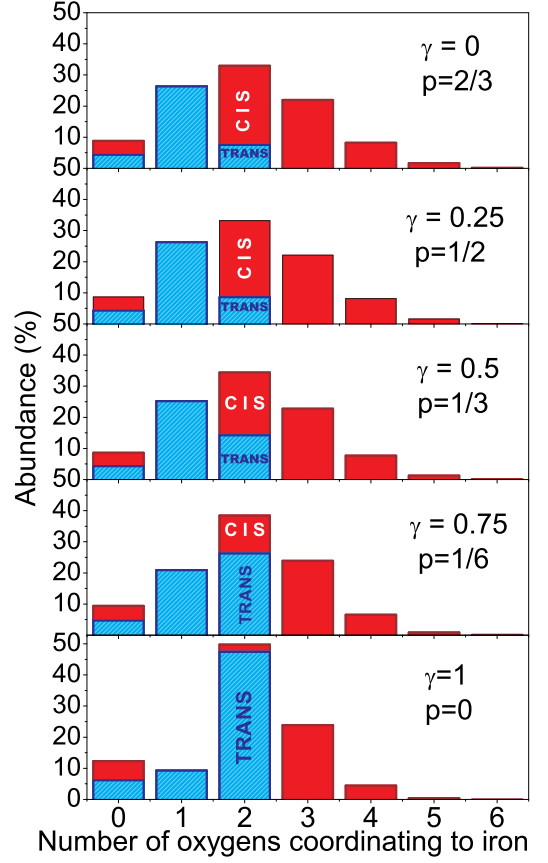


FIG. 7: Evolution of the distribution of abundances of the coordination polyhedra $\text{FeN}_{1-n}\text{O}_n$ ($n = 0, 1, 2, 3, 4, 5, 6$) as the structure randomizes starting from order parameter $\gamma = 1$ ($\text{Pm}\bar{3}\text{m}$ model, Fig1,b) to $\gamma = 0$ ($\text{Fm}\bar{3}\text{m}$ model, Fig.1 d). Here $p = 2(1 - \gamma)/3$ is the occupancy of the center of the cubic cell in Fig.1 (b). Total abundances of orbital singlet and orbital doublet ground states are distinguished by color.

6. Alkali-free ferrous cobalticyanide

The isomer shifts in the Mössbauer spectrum of the A-free $\text{Fe}[\text{Co}(\text{CN})_6]_{2/3}$ (Fig.6e) indicates predominantly (95% in best sample) the high-spin Fe^{2+} . The ground states of the major part of the Fe^{2+} species (64%) are the orbital singlet states. Second place in population is taken by the orbital doublet states. Third minor doublet is assigned to Fe^{3+} according to its isomer shift and magnetic measurements. Refinements of the structure of $\text{Fe}_{1.5}[\text{Co}(\text{CN})_6] \cdot \text{H}_2\text{O}$ were useful to confirm the assignments of three Fe^{2+} Mössbauer subspectra to the defined structural sites.

Let us consider first the structure models of archetype Prussian Blue investigated previously^{26,48}. The concentration of pores in the A-free hexacyanocobaltate is very large, therefore, the pores cannot be considered as isolated ones. All kinds of associations between the water-

filled pores underlie the resulting abundance of the Fe^{2+} species in various coordinations. Interactions between the pores at the stage of synthesis may result in various distributions of the pores. For the Prussian Blue $\text{Fe}_4[\text{Fe}(\text{CN})_6]_3 \cdot 14\text{H}_2\text{O}$, depending on the growth conditions, Buser et al²⁶ could synthesize the single crystals with varied degree of disorder. Structures of several crystals were refined using the $\text{Fm}\bar{3}\text{m}$ model, others were best refined using the $\text{Pm}\bar{3}\text{m}$ model. *A priori*, fully randomized distribution of the pores is consistent with the $\text{Fm}\bar{3}\text{m}$ model (Fig. 1d). Low symmetry ($\text{Pm}\bar{3}\text{m}$) becomes applicable when one finds unequal occupancies for the cell body center and edge centers (Fig. 1b). These sites are abundant with the ratio of 1:3. If p is the occupancy of the body center, and $1 - p/3$ is the occupancy of the edge centers, the conditions $p = 0$ and $p = 3/4$ correspond to fully ordered and random PB structures, respectively²⁶. In ferrous hexacyanocobaltate, owing to different valence ratio the same conditions correspond to $p = 0$ and $p = 2/3$. Intermediate partially-ordered structures can be characterized by the order parameter $\gamma = 1 - 3p/2$.

As γ decreases, the integral value of A_D shows in Fig. 7 the percentages of 63%, 52%, 44%, 39% and 38% for $\gamma = 1, \frac{3}{4}, \frac{1}{2}, \frac{1}{4}, 0$, respectively. Main trend of reduction of A_D is determined by the reduction of the *trans*-subpopulation of $\text{FeN}_4(\text{H}_2\text{O})_2$. The orbital singlet ground state prevails in the disordered structure described by the $\text{Fm}\bar{3}\text{m}$ model. In this case ($\gamma = 0$), the expected area of the external doublet A_S reaches the value of 62% similar to experimental result of 64% in Table IV.

In Fig. 7, we have calculated the abundance of various coordinations of Fe^{2+} for several values of γ between 0 and 1. The total abundance of the Fe^{2+} species in the orbital doublet ground state A_D is made up mainly of the abundances of $\text{FeN}_5\text{H}_2\text{O}$ and *trans*- $\text{FeN}_4(\text{H}_2\text{O})_2$. Relatively small number of water-free octahedra FeN_6 is assumed to be halved between two distortion isomers.

Abundance of the orbital singlet A_S is composed *cis*- $\text{FeN}_4(\text{H}_2\text{O})_2$, $\text{FeN}_3(\text{H}_2\text{O})_3$ and remaining FeN_6 (distortion isomer). Both in-plane and 3D ligand configurations in the 3:3 octahedron $\text{FeN}_3(\text{H}_2\text{O})_3$ contribute to A_S . First, when 3 oxygens coordinating to iron are in one plane the x , y and z axes become all nonequivalent. In this case, the spin-down electron cloud loses the axial symmetry, and the t_{2g} group splits into three singlets. Second, when three oxygens are in 3D configurations, all three axes x , y and z are equivalent; nevertheless, the cubic symmetry is lost. Since H_2O is a weaker ligand than N this geometry can be viewed as an octahedron with three ligands expelled to longer distance than other three. Equivalent spatial distortion is the elongation along the trigonal axis. Such a distortion was shown to stabilize the orbital singlet lowest¹².

While there are just two sorts of the ground states, the inspection of Fig.7 for $p=2/3$ shows that there are eight sites of Fe^{2+} having different ligand configurations with the abundance of 5% or more. Among the octahedra with

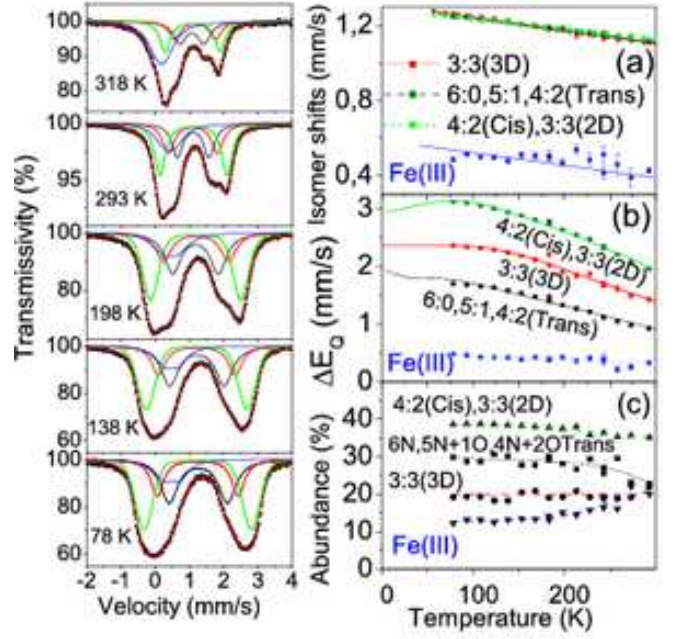


FIG. 8: Left panel: Mössbauer spectra of $\text{Fe}[\text{Co}(\text{CN})_6]_{0.67} \cdot 5\text{H}_2\text{O}$ at 78, 138, 198, 293 and 318 K fitted with four quadrupole doublets. The external (green color) doublet is assigned to Fe^{2+} (orbital singlet) inside the octahedra $\text{FeN}_4(\text{H}_2\text{O})_2$ with two H_2O in *cis*-conformation and $\text{FeN}_3(\text{H}_2\text{O})_3$ with three H_2O in one plane (2D conformation). Middle doublet (red color) is assigned to the orbital singlet ground state inside the $\text{FeN}_3(\text{H}_2\text{O})_3$ polyhedra with waters in 3D conformation. Inner Fe^{2+} doublet is associated with the FeN_6 , $\text{FeN}_5\text{H}_2\text{O}$, and *trans*- $\text{FeN}_4(\text{H}_2\text{O})_2$ polyhedra all favoring the orbital doublet states. The spectra below 293 K are reversible. Additional doublet (blue) has the isomer shift of Fe^{3+} . The spectra below 293 K are reversible. The sample warmed up to 318 K (uppermost spectrum) is changed irreversibly (for further details see text in Sec. III D). Right panel: temperature dependencies of the fit parameters of four quadrupole doublets: isomer shifts (a), quadrupole splittings (b) and abundances. Quadrupole splittings in (b) are fitted with the reduction factors $F'(T)$ from Ref.³⁷. The solid lines represent the theoretical $\Delta E_Q(T)$ for $\lambda = 58 \text{ cm}^{-1}$, $\Delta_1 = \Delta_2 = 320 \text{ cm}^{-1}$ for the external doublet attributed to the 4:2 (Cis) and 3:3 (2D) sites; $\lambda = 80 \text{ cm}^{-1}$, $\Delta_1 = \Delta_2 = 300 \text{ cm}^{-1}$ for the intermediate doublet attributed to the 3:3 (3D) site; $\lambda = 45 \text{ cm}^{-1}$, $\Delta_1 = 150 \text{ cm}^{-1}$, $\Delta_2 = 0$ for the internal doublet attributed to the 6:0, 5:1 and 4:2(Trans) sites.

$n=0,1,2,3$ and 4 those with $n=0, 2$ and 3 are found in two isomeric configurations: compression-elongation ($n=0$), *cis-trans* ($n=2$) and 2D-3D ($n=3$). These eight sites are to be completed with ninth site if the oxidized component (Fe^{3+}) is present in the sample. It appears that the most sophisticated way of spectra evaluation consist of partitioning the spectral area into nine doublets. Even if the method would reproducibly fit the multiple spectra, it would be uneasy task to assign the resulting subspec-

tra to a particular isomer. Highly valuable remains the models in which less than nine subspectra are assumed. In the A-free cobalticyanide (Fig.8), a plausible model of 4 subspectra is constructed through breaking up the external doublet with the excessive linewidth into two doublets. Resulting intermediate quadrupole doublet is assigned to the 3-dimensional 3:3 configuration of the ligands (3N+3H₂O). Corresponding crystal fields have a trigonal symmetry axis. We estimate this symmetry to reduce slightly the ensuing quadrupole splitting. Thus, in this model, the orbital singlet states stabilized in the crystal fields of trigonal symmetry are distinguished from the orbital singlet settled in the 4:2 (cis) and 3:3 (2D) environments.

In the experiment with enriched sample of ⁵⁷Fe[Co(CN)₆]_{0.67} · 5H₂O the spectra were collected with the step $\Delta T = 15$ K (Fig.8) The evaluation of these spectra with five, and six doublets were also attempted. These preliminary analyses showed that the model of four doublets, while providing already strong improvement of χ^2 , ensures also the most reproducible and stable solution. The model is changing its parameters smoothly as temperature changes.

Orbital ground state reversal observed above in the A-filled compounds (Fig.5) is not seen in the A-free ones (Fig.8). This is naturally explained by the small contribution of the n=0 sites susceptible to the distortion isomerism. It is shown in Fig.7 that the number of such sites does not exceed 8%. Other sites strongly perturbed by the CN ligand replacement exhibits persistent ground states independent of temperature.

Parameters of crystal-field splitting and spin-orbit coupling derived from fitting the temperature dependencies of ΔE_Q are in agreement with the averaged curve of $\mu_{\text{eff}}(T)$ on Fig. 3. The splitting of 340 cm⁻¹ estimated previously in Fe₃[Co(CN)₆]₂ · 5H₂O by Rasmussen and Meyers²⁰ corresponds closely to one of our results, namely, to the crystal fields in the Fe²⁺ sites contributing to the external doublet.

C. Models of short-range order in PB analogues

The concentration of pores in archetypal Prussian Blue, ferric ferrocyanide Fe[Fe(CN)₆]_{1- δ} · 3.5H₂O, is $\delta = 1/4$, so that the ratio $1 - \delta : \delta$ is 3: 1. The ordered Pm $\bar{3}$ m structure proposed for Prussian Blue in Ref.²⁶ contains the high-spin cations only in coordinations FeN₆ (25%) and trans-FeN₄(H₂O)₂ (75%). In ferrous hexacyanocobaltate, the ratio $1 - \delta : \delta$ is 2: 1. Therefore, for a vacancy-ordered phase of such a stoichiometry one cannot expect the same set of coordinations as for the Pm $\bar{3}$ m structure of the Ref.²⁶.

In order to construct an ordered phase with the ratio $1 - \delta : \delta$ of 2: 1 we try to fill 3 sites with Fe, 2 sites with Co, 1 site with Co vacancies, and 0 sites with Fe vacancies. We find that among cubic structures of NaCl-type there is no superstructure with exact site ra-

tio 3:2:1:0, however, a unique superstructure with the ratio of 30:20:12:2 exists. Using the body-centered Im $\bar{3}$ m model we can develop the proper arrangement of the vacancies with a variable order parameter. Table V shows the details of the fully ordered ($\gamma = 1$) Im $\bar{3}$ m structure. The order parameter $\gamma = 1 - 8p/3$ is defined via the occupancy p of the (12e) position that is the core of complex anion [Co(CN)₆]³⁻.

Table V. Wyckoff positions, atom type, relative coordinates and occupancies of the Na and Cl nodes in the superstructure Im $\bar{3}$ m model on the basis NaCl-type framework.

Wyckoff	Atom	x	y	z	Occ.
2a	Fe	0	0	0	0
6b	Fe <i>Trans</i>	0	1/2	1/2	1
8c	Co	1/4	1/4	1/4	1
12d	Co	1/4	0	1/2	1
12e	Co	1/4	0	0	0
24h	Fe <i>Cis</i>	0	1/4	1/4	1

Among total 14 vacancies per cubic cell of the Im $\bar{3}$ m structure (Table V) we place 12 vacancies of the complex anion Co(CN)₆ and 2 cationic (Fe²⁺) vacancies. We obtained the ordered structure of Fe[Co(CN)₆]_{2/3} · $\frac{85}{16}$ H₂O which contains 2 very large cross-shaped pores (6+1-pores, or +-pores). Each cationic vacancy is surrounded by 6 anionic vacancies. The hydration degree $\frac{85}{16}$ is calculated assuming 14 water molecules per standard pore and an additional water molecule per Fe²⁺ vacancy. Thus, the 6+1-pore is composed of 6 standard pores aggregated into 3D crosslike body. The edge of the Im $\bar{3}$ m cell is twice longer than the edge of the Pm $\bar{3}$ m cell and the cell volume is 8-fold.

The body-centered Im $\bar{3}$ m model exhibits only two kinds of Fe²⁺ sites with the abundance ratio of 3:1, similar to that of the Pm $\bar{3}$ m model. In both models, the major site (75%) is coordinated with two waters. However, in the Pm $\bar{3}$ m model the major site is coordinated by waters in *trans*-conformation, whereas in the Im $\bar{3}$ m model the major site is coordinated by waters in *cis*-conformation. The minor site in Pm $\bar{3}$ m model is coordinated by six nitrogens, and in Im $\bar{3}$ m model by four nitrogens and two waters in *trans*-conformation.

It is important that we were able to construct the superstructure model, which strongly favors the *cis*-conformation in agreement with prevailing external doublet in Mössbauer spectra. Although the random Fm $\bar{3}$ m model agrees as well with the experiment, the lack of any short-range order between pores appears to be a severe limitation of this model because the vacancies bearing a charge interact with each other repulsively. We must note also that the lack of any superstructure reflections in diffraction patterns may not be an evidence of a missing short-range order, but only the evidence of lacking *long-range* order. The suggested Im $\bar{3}$ m structure is a plausible model of the short-range order in the mixed-valence 2:3 PB analogues.

Although the superstructure reflections, predicted by either Pm $\bar{3}$ m or Im $\bar{3}$ m models, were not observed by x-

ray diffraction, using the probabilities of local structure patterns observed by such a local technique as Mössbauer spectroscopy one can identify the proper model of short-range order. The $\text{Im}\bar{3}\text{m}$ model predicts the strong predominance (3:1) of *cis*- over *trans*- population among the Fe^{2+} environments. The model describes the situation when concentration of elementary vacancies is so high that they must be in small clusters. In contrast, the $\text{Pm}\bar{3}\text{m}$ model describes the limit when all vacancies are still isolated, however, no more vacancies can be added without clustering. If they are actually added to proceed from $\delta = 1/4$ to $\delta = 1/3$ (as in the bottom panel of Fig.7), there will result the extra-hole $\text{Pm}\bar{3}\text{m}$ model that fails to describe the Mössbauer spectral data. In our experiments, we observe the prevailing abundance of the *cis*-conformations related to the extended crosslike pores. The aggregation of small pores into extended pores underlies the large (up to $750 \text{ m}^2/\text{g}$) specific surface and unique gas sorption properties of these materials⁴⁹.

D. Charge-transferred states in the PB analogues

The charge-transferred states which were discussed above to induce the distortion isomerism are seen in the third small doublet with IS of Fe^{3+} in Figs. 6 (c,e) and 8. A slight asymmetry appears also in spectra of Fig.4, although these spectra can be just a little less well fitted without introducing explicitly the Fe^{3+} component. The pairs of $\text{Fe}^{2+}/\text{Co}^{3+}$ and $\text{Fe}^{3+}/\text{Co}^{2+}$ can be considered as valence tautomers, and we explain the asymmetry in these spectra by electron transfer from Fe^{2+} to Co^{3+} . The formation and rupture of the chemical bonds implies no migration of atoms but only migration of electrons. The cobalt ions remain in low-spin state as the sixth electron of Fe^{2+} transfers from t_{2g} orbital of Fe^{2+} to e_g orbital of Co^{2+} . Other compound susceptible to valence tautomerism were known previously^{27,50}. For example, the Prussian Blue analogue $\text{RbMn}[\text{Fe}(\text{CN})_6] \cdot \text{H}_2\text{O}$, when synthesized in Rb excess that fills enough framework interstitials with Rb, crystallizes in the structure shown in Fig. (1a). In this system, the tautomers $\text{Fe}^{2+}/\text{Mn}^{3+}$ and $\text{Fe}^{3+}/\text{Mn}^{2+}$ are able to form different crystal phases which give way to each other as temperature changes.

In the ferrous cobalticyanides, no abrupt phase change was found to be caused by the charge-transferred states. On the other hand, we observed that the content of Fe^{3+} can be changed depending on the excess of FeCl_2 and dilution degree in the course of precipitation of $\text{Fe}[\text{Co}(\text{CN})_6]_{2/3} \cdot 5\text{H}_2\text{O}$. Rapidly synthesized isotope-enriched compound contained up to 15-20% of Fe^{3+} , however, the content of Fe^{3+} was reduced down to just 5% through reducing the reaction rate in dilute solutions. Most probably, the lack or misplacement of water molecules is needed to stabilize locally the charge-transferred states and make them observable in Mössbauer spectra. It appears in this case that the

rapidly prepared samples are not saturated in C-water. The sites of Fe^{2+} nearest to the nodes lacking the coordination water are subject of local tautomer transformation. In a slowly synthesized $\text{Fe}_{1.5}[\text{Co}(\text{CN})_6] \cdot 5\text{H}_2\text{O}$ such crystallization defects are reduced.

Measuring the Mössbauer spectra above room temperature supports this concept. With raising temperature the area of the Fe^{3+} subspectrum starts to increase irreversibly. Thermogravimetric analysis showed that the loss of sample weight occurs at heating practically starting from room temperature. The Mössbauer spectrum measured *in situ* in a furnace at 318 K shows the area of the Fe^{3+} doublet increased up to 37%. The same sample measured *ex-situ* after prolonged (1 week) heat treatment at 60°C showed the area of the Fe^{3+} increased up to 57%. The equilibrium hydration degree at 60°C is related with nearly half iron species transformed to Fe^{3+} . Longer exposure in air at 60°C induces no further increase of the spectral asymmetry and the area of spectral component with IS of 0.39 mm/s remains at the level of 60%.

The isomer shift of 0.39 mm/s is attributable, in principle, either to high-spin Fe^{3+} or to low spin Fe^{2+} . The latter was observed below the spin-state transition in $\text{CsFe}[\text{Cr}(\text{CN})_6]^{23}$. Theoretical approaches to lattice-dynamic calculations^{51,52} show that the change in the electronic state is closely related to the structure expansion as the lattice parameter grows between the low-spin and high-spin forms from 1.03 nm to 1.07 nm . In $\text{Fe}_3[\text{Co}(\text{CN})_6]_2 \cdot n\text{H}_2\text{O}$, the thermal lattice expansion is negative⁴³. To verify that we do not deal with a *reverse* spin transition^{53,54}, we have compared the magnetic susceptibilities of the samples having 5% and 57 % of the subspectrum with IS of 0.39 mm/s . In the heat-treated sample, the susceptibility increased too little compared to what is expected for the increase of μ_{eff} upto $5.9 \mu_{\text{B}}$. With the weight loss taken into account this result would rather indicate the formation of an intermediate-spin state of Fe^{3+} which is known for strongly distorted octahedral coordinations with two alternate ligands in *cis*-configuration⁵⁵.

IV. CONCLUSION

Mössbauer spectroscopy was applied to study the mixed-valence ($\text{Fe}^{2+}\text{-Co}^{3+}$) PB analogues which displayed the mixed-orbital ground states of Fe^{2+} ions. The ground state mixing originates from both the distortion isomerism and the varied composition of Fe^{2+} nearest-neighbor environment. In the A-free PB analogues, water molecules enter the first coordination sphere of the Fe^{2+} ions. There appears two kinds of anisotropic ligand configurations which are the intrinsic generant of the singlet and doublet orbital ground states. The Fe^{2+} sites are thus classified into two types.

Distribution of the anionic vacancies (water-filled pores) over the framework is characterized by the order parameter for two long-range order models $\text{Pm}\bar{3}\text{m}$ or

$\text{Im}\bar{3}\text{m}$. These models are relevant to the PB analogues of the 4:3 and 3:2 stoichiometries, respectively. Two water molecules within the first coordination sphere of Fe^{2+} is the most populated configuration of the random model $\text{Fm}\bar{3}\text{m}$ and ordered models $\text{Pm}\bar{3}\text{m}$ or $\text{Im}\bar{3}\text{m}$. The short-range order event occurrence in PB analogues of the 3:2 and 4:3 stoichiometries favors the cis- and trans- conformations, respectively. Orbital singlet is the lowest in energy state for the cis-conformation. Accordingly, in the A-free ferrous cobalticyanide PB analogue, the Mössbauer spectra of Fe^{2+} are dominated by the larger quadrupole-splitting component.

In the A-filled PB analogues, where the the water ligands are withdrawn from the Fe^{2+} coordination sphere, the least anisotropic charge distribution attainable for the cases of $\text{A}=\text{Rb}$ and Cs is the orbital doublet ground state. For $\text{A}=\text{Na}$ and K , the thermally-induced interconversions between the doublet and singlet ground states were observed attributed to distortion isomerism. Charge-transferred states intrinsic in the PB analogues with negative thermal expansion³⁹ are suggested to be the source of the lattice distortions associated with the distortion isomerism. Asymmetry of Mössbauer spectra is attributed to the admixture of a small content (at the level of $\sim 5\%$) of the Fe^{3+} species associated with the charge-transferred states.

Since the octahedral sites FeN_6 possess a higher sym-

metry than the sites $\text{FeN}_{6-n}(\text{H}_2\text{O})_n$ we observe upon the insertion the A-ions into A free compounds that the value of Mössbauer QS drops in ferrous cobalticyanides similarly to the archetypal Prussian Blue $\text{Fe}_4[\text{Fe}(\text{CN})_6]_3 \cdot 14\text{H}_2\text{O}$ ²⁸. However, when the large-size A-ions (Cs , Rb) replace the small-size ones (Na , K) through ionic exchange we observe the larger QS associated with lower symmetry local distortion isomer; the sixth d-electron of the Fe^{2+} cation is self-localized on a single sublevel (orbital singlet) of the t_{2g} group owing to strong lattice distortions around the implanting sites of the low-mobility ions.

V. ACKNOWLEDGEMENT

This work was partly supported by the Chinese Academy of Sciences Visiting Professorships for Senior International Scientists. Grant No. 2011T1G15. Financial support obtained from the Chinese Academy of Sciences for “100 Talents” Project, the National Natural Science Foundation of China (No. 11079036) and the Natural Science Foundation of Liaoning Province (No. 20092173) is also greatly acknowledged.

-
- ¹ K. Kato, Y. Moritomo, M. Takata, M. Sakata, M. Umekawa, N. Hamada, S. Ohkoshi, H. Tokoro, and K. Hashimoto, *Phys. Rev. Lett.* **91**, 255502 (2003).
 - ² Ph. Gülich, Y. Garcia, and H.A. Goodwin, *Chem. Soc. Rev.* **29**, 419-427 (2000).
 - ³ E. Coronado, M.C. Giménez-López, T. Korzeniak, G. Levchenko, F.M. Romero, A. Segura, V. García-Baonza, J.C. Cezar, F.M.F. de Groot, A. Milner, and M. Paz-Pasternak, *J. Am. Chem. Soc.* **130**, 15519-15532 (2008).
 - ⁴ C. Chong, M. Itoi, K. Boukheddaden, E. Codjovi, A. Rotaru, F. Varret, F.A. Frye, D.R. Talham, I. Maurin, D. Chernyshov, and M. Castro, *Phys. Rev. B* **84**, 144102 (2011).
 - ⁵ A. B. Koudriavtsev, W. Linert, *J. Struct. Chem. Engl. Transl.* **51**, 335-365 (2010).
 - ⁶ Y. Moritomo, F. Nakada, H. Kamioka, T. Hozumi, and S. Ohkoshi, *Phys. Rev. B* **75**, 214110 (2007).
 - ⁷ M. Kabir and K.J. VanVleet, *Phys. Rev. B* **85**, 054431 (2012).
 - ⁸ A.I. Rykov, Y. Ueda, K. Nomura, and M. Seto, *Phys. Rev. B* **79** 224114 (2009).
 - ⁹ I. Dézsi and L. Keszthelyi, *Solid St. Comm.* **4**, 511 (1966).
 - ¹⁰ J. M. D. Coey, I. Dézsi, P. M. Thomas, and P.J. Ouseph, *Phys. Lett.* **41A**, 125 (1972).
 - ¹¹ W.M. Reiff, R.B. Frankel, C.R. Abeledo, *Chem. Phys. Lett.* **22**, 124 (1973).
 - ¹² R. Latorre, C.R. Abeledo, R.B. Frankel, J.A. Costamagna, W.M. Reiff, E. Frank, *J. Chem. Phys.* **59**, 2580-2585(1973).
 - ¹³ R. Latorre, J.A. Costamagna, E. Frank, C.R. Abeledo, and R.B. Frankel, *J. Physique (Paris)* **C6**, 635 (1974).
 - ¹⁴ R. Latorre, J.A. Costamagna, E. Frank, C.R. Abeledo, and R.B. Frankel, *J. Inorg. Nucl. Chem.* **41**, 649-655 (1979).
 - ¹⁵ U. Volland, S. Hösl, H. Spiering, I. Dézsi, T. Kemény, and D.L. Nagy, *Solid St. Comm.* **27**, 49 (1978).
 - ¹⁶ U. Volland, *J. Phys. Colloques*, **41**, C1-309-C1310 (1980).
 - ¹⁷ B. Brunot, *Chem. Phys. Lett.* **29**, 371 (1974).
 - ¹⁸ B. Brunot, *Chem. Phys. Lett.* **29**, 368 (1974).
 - ¹⁹ G.R. Hoy, and F. de. S. Barros, *Phys. Rev.* **139**, A929-A934 (1965).
 - ²⁰ P.G. Rasmussen and E.A. Meyers, *Polyhedron* **3** 183-190 (1984).
 - ²¹ E. Reguera, H. Yee-Madeira, S. Demeshko, G. Eckold, and J. Jimenez-Gallegos, *Z. Phys. Chem.*, **223**, 701-711(2009).
 - ²² E. Reguera, H. Yee-Madeira, J. Fernández-Bertran, L. Nuñez, *Transition Met. Chem.*, **24**, 163-167(1999).
 - ²³ W. Kosaka, K. Nomura, K. Hashimoto, and S.-I. Ohkoshi, *J. Am. Chem. Soc.* **127**, 8590 (2005).
 - ²⁴ J. F. Keggin, and F.D. Miles, *Nature (London)* **137**, 577-578(1936).
 - ²⁵ A. Ludi, H.U. Güdel, *Struct. Bonding*, **14** 1-21, (1973).
 - ²⁶ H.J. Buser, D. Schwarzenbach, W. Petter, and A. Ludi, *Inorg. Chem.* **16**, 2704-2710(1977).
 - ²⁷ H. Tokoro, S.-I. Ohkoshi, T. Matsuda and K. Hashimoto, *Inorg. Chem.* **43**, 5231-5236 (2004).
 - ²⁸ A.I. Rykov, J. Wang, T. Zhang and K. Nomura, *Hyperfine Interact.* DOI 10.1007/s10751-012-0705-5 (in press).
 - ²⁹ A.J. Nozik and M. Kaplan, *Phys. Rev.* **159**, 273 (1967).
 - ³⁰ R.J. Evans, D.G. Rancourt, and M. Grodzicki, *American Mineralogist* **90**, 187-198 (2005).

- ³¹ E. König and A.S. Chakravarty, *Theoret. Chim. Acta (Berl.)* **9**, 151–170 (1967).
- ³² B.N. Figgis, J. Lewis, F. Mabbs, and G.A. Webb, *Nature* **203**, 1138 (1964).
- ³³ E. König, A.S. Chakravarty, and K. Madeja, *Theoret. Chim. Acta (Berl.)* **9**, 171–181 (1967).
- ³⁴ B.N. Figgis, J. Lewis, F. Mabbs, and G.A. Webb, *J. Chem. Soc. (A)* 442–447 (1964).
- ³⁵ The results tabulated in the above works^{33,34} are reported with different conventions for the sign of crystal field splitting δ . We avoid using the negative numbers for the crystal-field splitting energy. Instead of $|\delta|$, and sign of δ we use explicitly the notations of Δ_1 and Δ_2 , such that $\Delta_1 = \Delta_2$ when orbital singlet is lowest, and $\Delta_2 = 0$, when the orbital singlet is lowest.
- ³⁶ U. Ganiel, *Chem. Phys. Lett.*, **4**, 87 (1969).
- ³⁷ R. Ingalls, *Phys. Rev.* **133**, A787–A795 (1964).
- ³⁸ P.B. Merrithew, P.G. Rasmussen, and D.H. Vincent, *Inorg. Chem.* **10**, 1401–1406 (1971).
- ³⁹ T. Matsuda, J.E. Kim, K. Ohoyama, and Y. Moritomo, *Phys. Rev. B* **79**, 172302 (2009).
- ⁴⁰ E. Mikuli, A. Migdal-Mikuli, and J. Mayer, *J. Thermal Anal.* **54**, 93–102 (1998).
- ⁴¹ C. Nöldeke, B. Asmussen, W. Press, H. Büttner, G. Kearley, R. E. Lechner and B. Rufflé, *J. Chem. Phys.* **113** (2000) 3219.
- ⁴² B.K. Chaudhuri, *Solid St. Comm.* **16**, 767–772 (1975).
- ⁴³ S. Adak, L.L. Daemen, M. Hartl, D. Williams, J. Summerhill, H. Nakotte, *J. Solid St. Chem.* **184**, 2854 (2011).
- ⁴⁴ M.W. Reiff, R.B. Frankel, B.F. Little, and G.J. Long, *Chem. Phys. Lett.* **28**, 68 (1974).
- ⁴⁵ A. Widmann, H. Kahlert, I. Petrovic-Prelevic, H. Wulff, J. V. Yakhmi, N. Bagkar, and F. Scholz, *Inorg. Chem.* **41** (2002) 5706–5715.
- ⁴⁶ S. Ayrault, B. Jimenez, E. Garnier, M. Fedoroff, D.J. Jones, and C. Loos-Neskovic, *J. Solid St. Chem.* **141**, 475–485 (1998).
- ⁴⁷ C. Loos-Neskovic, S. Ayrault, V. Badillo, B. Jimenez, E. Garnier, M. Fedoroff, D.J. Jones, and B. Merinov, *J. Solid St. Chem.* **177**, 1817–1828 (2004).
- ⁴⁸ F. Herren, P. Fischer, A. Ludi, and W. Hälg, *Inorg. Chem.* **19**, 956–959 (1980).
- ⁴⁹ S.S. Kaye, J.R. Long, *Catal. Today*, **120**, 311–316 (2007).
- ⁵⁰ V. Ksenofontov, A. B. Gaspar and P. Gülich, *Topics in Current Chemistry*, 2004, Volume 235, Spin Crossover in Transition Metal Compounds III, Pages 39–66.
- ⁵¹ J.C. Wojdeł, I.P.R. Moreira, and F. Illas, *J. Chem. Phys.* **130**, 014702 (2009).
- ⁵² D.S. Middlemiss, D. Portinari, C.P. Grey, C.A. Morrison, and C.C. Wilson, *Phys. Rev. B* **81**, 184410 (2010).
- ⁵³ S. Hayami, Y. Shigeyoshi, M. Akita, K. Inoue, K. Kato, K. Osaka, M. Takata, R. Kawajiri, T. Mitani, and Y. Maeda, *Angew. Chem. Int. Ed.* **44**, 4899 (2005).
- ⁵⁴ P.T. Manoharan, B. Sambandam, R. Amasarani, B. Varghese, C.S. Gopinath, and K. Nomura, *Inorg. Chem. Acta* **374**, 586 (2011).
- ⁵⁵ P.J. van Koningsbruggen, Y. Maeda, H. Oshio, *Top. Curr. Chem.* **233**, 259 (2004).